5ICEGE
5th International Conference on Earthquake Geotechnical Engineering
January 2011, 10-13 | Santiago, Chile
Paper No. ABASC

A BAYESIAN APPROACH TO THE DETERMINATION OF THE FK SPECTRUM IN SASW TESTS

Mattias SCHEVENELS[1], Geert DEGRANDE[2], Geert LOMBAERT[3]

ABSTRACT

This paper presents a Bayesian technique for the computation of the frequency-wavenumber (FK) spectrum of the wave field recorded in a multi-station Spectral Analysis of Surface Waves (SASW) test. The technique is based on a probability distribution for the wave field in the soil: a probability is assigned to any conceivable wave field, reflecting the degree of belief that it corresponds to the real wave field generated in the SASW test. First, a prior probability distribution is built: a prior stochastic soil model is defined, based on the prior knowledge of the soil properties, and a Monte Carlo simulation is performed where the wave field in the soil is computed for a large number of soil profiles. The wave field is calculated both in the frequency-space domain and in the frequency-wavenumber domain, and the correlation between both domains is computed. In the next step, a Bayesian approach is followed to update the prior probability distribution taking into account the data recorded in the SASW test. This results in a posterior probability distribution of the FK spectrum.

The proposed method is applied to a site in Heverlee (Belgium). The soil profile corresponding to the FK spectrum thus obtained is determined by means of a Markov chain Monte Carlo method. In order to verify the resulting soil profile, it is used to compute the transfer functions of the soil, which are confronted with the experimental transfer functions determined in the SASW test. A good correspondence is observed, indicating that the soil profile properly reflects the data obtained from the SASW test.

Keywords: SASW, FK spectrum, Bayesian updating, Kalman filter.

INTRODUCTION

The multi-station Spectral Analysis of Surface Waves (SASW) method is a technique to determine the dynamic properties of shallow soil layers (Nazarian and Desai; 1993; Yuan and Nazarian; 1993). The SASW method has originally been developed for the determination of the dynamic shear modulus of the soil, but is now also used to estimate the material damping ratio (Lai; 1998; Rix et al.; 2000; Badsar et al.; 2010). The method has been used in various applications over the past couple of decades, such as the investigation of pavement systems (Nazarian and Stokoe II; 1984), the quality assessment of ground improvement (Cuellar and Valerio; 1997), the determination of the thickness of waste deposits (Kavazanjian et al.; 1994), and the identification of the dynamic soil properties for the prediction of ground vibrations (Lombaert et al.; 2006).

The SASW method is based on an in situ experiment where surface waves are generated by means of an impact hammer, a falling weight, or a hydraulic shaker. The resulting wave field is recorded by a large number of accelerometers or geophones along a straight measurement line at the soil surface. This wave field is dominated by dispersive surface waves. The dispersion and attenuation curves, representing the frequency dependent phase velocity and spatial decay of the surface waves, are determined from the

[1]Postdoctoral fellow, Department of Civil Engineering, K.U.Leuven, Belgium, e-mail: mattias.schevenels@bwk.kuleuven.be.
[2]Professor, Department of Civil Engineering, K.U.Leuven, Belgium, e-mail: geert.degrande@bwk.kuleuven.be.
[3]Professor, Department of Civil Engineering, K.U.Leuven, Belgium, e-mail: geert.lombaert@bwk.kuleuven.be.

measurement data. An inverse problem is finally solved in order to obtain a soil profile that matches the experimental dispersion and attenuation curves.

The dispersion and attenuation curves of the soil are often determined by means of the frequency-wavenumber (FK) spectrum of the wave field. A variety of methods is available to compute the FK spectrum, but all methods are essentially based on the application of an integral transformation. In this transformation, the wave field is usually linearly interpolated between the sensor locations, and the integral is truncated to the array length. The interpolation leads to aliasing errors in the high wavenumber range, while the truncation leads to a loss of resolution in the low wavenumber range.

The use of dispersion and attenuation curves in the SASW method implies that the experimental data are only partially taken into account. Forbriger 2003a; 2003b proposes an alternative procedure based on the inversion of the complete FK spectrum, so exploiting the full signal content available from the SASW test. Forbriger's inversion procedure hinges on the assignment of the proper weighting factors to different portions of the FK spectrum, as the accuracy of the spectrum is strongly variable due to factors such as measurement noise and the lack of resolution. In order to obtain satisfactory results, manual adjustments of the weighting factors are repeatedly required, making the inversion procedure a time consuming task.

This paper presents a Bayesian approach (Bayes; 1763) for the determination of the FK spectrum. First, a prior probability distribution for the wave field in the soil is formulated: a prior stochastic soil model is defined, based on the prior knowledge of the soil properties, and a Monte Carlo simulation is performed to obtain the corresponding wave field in the soil. The wave field is calculated both in the frequency-space domain and in the frequency-wavenumber domain, and the correlation between both domains is computed. Only the second order characteristics of the wave field are withheld and the wave field is assumed to follow a Gaussian distribution. Next, the prior probability distribution is updated accounting for the data recorded in the SASW test. The assumption of a Gaussian distribution allows for the use of an analytical technique, i.e. the Kalman filter, to perform the Bayesian updating procedure. This results in a posterior probability distribution for the wave field, both in the frequency-space domain and in the frequency-wavenumber domain. From a probabilistic point of view, this probability distribution is the solution to the problem of determining the FK spectrum. If a single deterministic solution is required, the FK spectrum with maximum posterior probability should be considered.

The method has two advantages compared to the integral transformation methods: (1) it leads to a more realistic estimate of the FK spectrum as no interpolation or truncation of the data is performed, and (2) the result is a complete stochastic characterization of the wave field in the soil, i.e. both the mean FK spectrum and its (co)variance are obtained. The variance of the FK spectrum can be used to determine the proper weighting factors in a deterministic inversion procedure such as the method proposed by Forbriger 2003b, so avoiding the need for manual interventions. Alternatively, stochastic inversion methods can be used to determine the entire ensemble of soil profiles that correspond to the FK spectrum.

The paper is organized as follows. The first section focuses on an SASW test performed in Heverlee (Belgium) and describes the determination of the transfer functions from the source (an impact hammer) to the receivers in the free field. The second section addresses the determination of the posterior probability distribution of the FK spectrum. The corresponding soil profile is determined in the third section, using a stochastic inversion scheme based on a Markov chain Monte Carlo technique (Mosegaard and Tarantola; 1995). In the fourth section, the resulting soil profile is verified: the transfer functions for this soil profile are computed and confronted with the experimental data presented in the first section.

SASW TEST

An SASW test performed on a site in Heverlee is considered. This test has been performed as a part of a study to determine the most appropriate site for a nanotechnology facility on the K.U.Leuven campus (Schevenels and Degrande; 2009).

The Database of the Subsoil of Flanders (Databank Ondergrond Vlaanderen) describes a number of borings performed on or close to the measurement site. According to boring kb32d89e-B304, performed in 1974, the soil at this site consists of a disturbed surface layer with a thickness of $0.6\,\mathrm{m}$, layers of peat, loam, and clay upto a depth of $10\,\mathrm{m}$, a layer of sand upto a depth of $12\,\mathrm{m}$, layers of gravel upto a depth of $14\,\mathrm{m}$, and a layer of tertiary sand upto a depth of $95\,\mathrm{m}$.

In the SASW test performed in Heverlee, surface waves are generated by means of a hammer impact on a small aluminum foundation. The impact force has been recorded by means of a force sensor integrated in the hammer. The response has been measured by $N_\mathrm{S} = 40$ accelerometers located between $1\,\mathrm{m}$ and $80\,\mathrm{m}$ from the source, separated by $1\,\mathrm{m}$ in the near field up to $4\,\mathrm{m}$ in the far field.

The wave field recorded in the SASW test is contaminated by noise. To mitigate the influence of the noise, the test is repeated a large number of times (i.e. the response from multiple hammer impacts is recorded) and the average transfer function from the hammer force to the free field acceleration is computed. In the present test, $N_\mathrm{I} = 85$ hammer impacts have been performed.

First, the auto power spectral densities of the force and the response and the cross power spectral densities between force and response are determined:

$$\hat{s}_\mathrm{i}(\omega) = \frac{1}{N_\mathrm{I}} \sum_{k=1}^{N_\mathrm{I}} \hat{f}_k(\omega) \hat{f}_k^*(\omega) \tag{1}$$

$$\hat{\mathbf{s}}_\mathrm{o}(\omega) = \frac{1}{N_\mathrm{I}} \sum_{k=1}^{N_\mathrm{I}} \hat{\mathbf{a}}_k(\omega) \hat{\mathbf{a}}_k^\mathrm{H}(\omega) \tag{2}$$

$$\hat{\mathbf{s}}_\mathrm{io}(\omega) = \frac{1}{N_\mathrm{I}} \sum_{k=1}^{N_\mathrm{I}} \hat{f}_k(\omega) \hat{\mathbf{a}}_k^\mathrm{H}(\omega) \tag{3}$$

$$\hat{\mathbf{s}}_\mathrm{oi}(\omega) = \frac{1}{N_\mathrm{I}} \sum_{k=1}^{N_\mathrm{I}} \hat{\mathbf{a}}_k(\omega) \hat{f}_k^*(\omega) \tag{4}$$

where N_I is the number of hammer impacts, $\hat{f}_k(\omega)$ is the frequency content of the force for impact k, and $\hat{\mathbf{a}}_k(\omega)$ is a vector collecting the frequency content of the acceleration at all receivers for impact k. An asterisk denotes the complex conjugate of a scalar and a subscript H denotes the Hermitian of a vector.

Next, the H_1 estimator (Ewins; 1984) is used to determine the average transfer function from the force to the free field acceleration:

$$\hat{\mathbf{h}}_\mathrm{e}(\omega) = \frac{\hat{\mathbf{s}}_\mathrm{oi}(\omega)}{\hat{s}_\mathrm{i}(\omega)} \tag{5}$$

The vector $\hat{\mathbf{h}}_\mathrm{e}(\omega)$ collects the average transfer functions for all receivers.

Due to the presence of noise, the transfer function $\hat{\mathbf{h}}_\mathrm{e}(\omega)$ obtained with the H_1 estimator is a random variable, in the sense that each experiment gives rise to a different estimation. The transfer function $\hat{\mathbf{h}}_\mathrm{e}(\omega)$ can therefore be decomposed as follows:

$$\hat{\mathbf{h}}_\mathrm{e}(\omega) = \mathbf{m}_{\hat{\mathbf{h}}_\mathrm{e}}(\omega) + \Delta\hat{\mathbf{h}}_\mathrm{e}(\omega) \tag{6}$$

where $\mathbf{m}_{\hat{\mathbf{h}}_\mathrm{e}}(\omega)$ is the true value of the transfer function and $\Delta\hat{\mathbf{h}}_\mathrm{e}(\omega)$ is the measurement error due to the presence of noise.

Assuming that the noise is stationary and uncorrelated for different hammer impacts, the covariance matrix $\mathbf{C}_{\hat{\mathbf{h}}_\mathrm{e}}(\omega)$ of the transfer function $\hat{\mathbf{h}}_\mathrm{e}(\omega)$ can be estimated as (Cauberghe; 2004):

$$\mathbf{C}_{\hat{\mathbf{h}}_\mathrm{e}}(\omega) = \frac{1}{N_\mathrm{I}\hat{s}_\mathrm{i}(\omega)} \left(\hat{\mathbf{s}}_\mathrm{o}(\omega) - \mathbf{h}_\mathrm{e}(\omega)\hat{\mathbf{s}}_\mathrm{io}(\omega)\right) \tag{7}$$

The variance $\boldsymbol{\sigma}^2_{\hat{\mathbf{h}}_\mathrm{e}}(\omega)$ of the estimated transfer function is given by:

$$\boldsymbol{\sigma}^2_{\hat{\mathbf{h}}_\mathrm{e}}(\omega) = \mathrm{diag}\left(\mathbf{C}_{\hat{\mathbf{h}}_\mathrm{e}}(\omega)\right) \tag{8}$$

A low value of the standard deviation $\boldsymbol{\sigma}_{\hat{\mathbf{h}}_\mathrm{e}}(\omega)$ indicates an accurate estimation of the transfer function. Equations (7) and (8) show that the variance $\boldsymbol{\sigma}^2_{\hat{\mathbf{h}}_\mathrm{e}}(\omega)$ is inversely proportional to the number of impacts N_I. As a result, the accuracy of the estimation increases proportionally to $\sqrt{N_\mathrm{I}}$.

In order to save computer memory, only a limited number of frequencies is used in the analysis: 40 frequencies are selected, ranging from $0.98\,\mathrm{Hz}$ to $78.13\,\mathrm{Hz}$, and separated by $0.98\,\mathrm{Hz}$ in the low frequency range up to $3.91\,\mathrm{Hz}$ in the high frequency range. The corresponding components of the transfer function $\hat{\mathbf{h}}_\mathrm{e}(\omega)$ are stored in a vector $\hat{\mathbf{H}}_\mathrm{e}$ of length $N_\mathrm{FS} = N_\mathrm{F}N_\mathrm{S}$, where $N_\mathrm{F} = 40$ is the number of frequencies and $N_\mathrm{S} = 40$ is the number of accelerometers:

$$\hat{\mathbf{H}}_\mathrm{e} = \begin{bmatrix} \hat{\mathbf{h}}_\mathrm{e}(\omega_1) \\ \hat{\mathbf{h}}_\mathrm{e}(\omega_2) \\ \vdots \\ \hat{\mathbf{h}}_\mathrm{e}(\omega_{\mathrm{N_F}}) \end{bmatrix} \tag{9}$$

The covariance matrix $\mathbf{C}_{\hat{\mathbf{H}}_\mathrm{e}}$ of the transfer function at the selected frequencies is constructed in a similar way:

$$\mathbf{C}_{\hat{\mathbf{H}}_\mathrm{e}} = \begin{bmatrix} \mathbf{C}_{\hat{\mathbf{h}}_\mathrm{e}}(\omega_1) & & & 0 \\ & \mathbf{C}_{\hat{\mathbf{h}}_\mathrm{e}}(\omega_2) & & \\ & & \ddots & \\ 0 & & & \mathbf{C}_{\hat{\mathbf{h}}_\mathrm{e}}(\omega_{\mathrm{N_F}}) \end{bmatrix} \tag{10}$$

This is a block diagonal matrix, reflecting the assumption of zero correlation between different frequencies.

The variance $\boldsymbol{\sigma}^2_{\hat{\mathbf{H}}_\mathrm{e}}$ of the transfer function at the the selected frequencies is given by the following vector:

$$\boldsymbol{\sigma}^2_{\hat{\mathbf{H}}_\mathrm{e}} = \mathrm{diag}\left(\mathbf{C}_{\hat{\mathbf{H}}_\mathrm{e}}\right) \tag{11}$$

Figure 1 shows the modulus of the transfer function $\hat{\mathbf{H}}_\mathrm{e}$ and the coefficient of variation $\boldsymbol{\sigma}_{\hat{\mathbf{H}}_\mathrm{e}}/|\hat{\mathbf{H}}_\mathrm{e}|$ for the site in Heverlee.

The modulus of the transfer function $\hat{\mathbf{H}}_\mathrm{e}$ in figure 1a decays with distance due to geometric and material damping. Material damping is frequency dependent, resulting in a stronger decay in the higher frequency range.

The coefficient of variation $\boldsymbol{\sigma}_{\hat{\mathbf{H}}_\mathrm{e}}/|\hat{\mathbf{H}}_\mathrm{e}|$ in figure 1c allows for the assessment of the data quality: the coefficient of variation is small in a frequency range with a lower bound of about $6\,\mathrm{Hz}$ and an upper bound that decreases with the distance from the source. In this frequency range, the data quality is good, as the signal-to-noise ratio is high. Outside this frequency range, the coefficient of variation increases, indicating a lower signal-to-noise ratio.

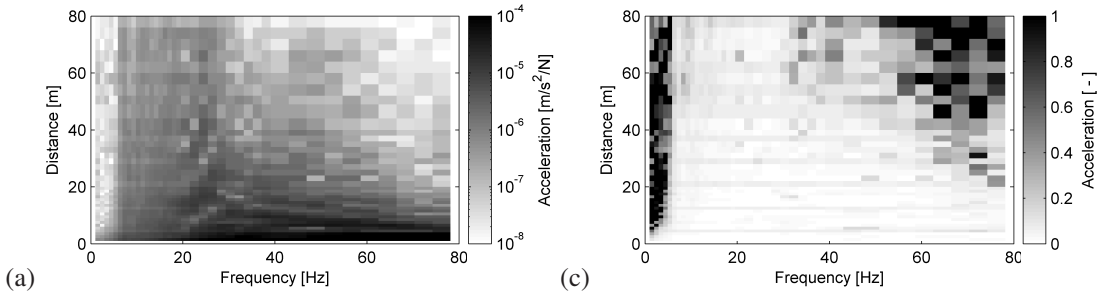

Figure 1. (a) Modulus $|\hat{\mathbf{H}}_{\mathrm{e}}|$ and (b) coefficient of variation $\sigma_{\hat{\mathbf{H}}_{\mathrm{e}}}/|\hat{\mathbf{H}}_{\mathrm{e}}|$ of the transfer function for the site in Heverlee.

FK SPECTRUM

A Bayesian approach is now followed to characterize the FK spectrum of the wave field in the soil. First, a prior stochastic model for the wave field in the soil is formulated. Next, this prior model is updated by means of a likelihood function defined using the experimental data described in the first section. This results in a posterior stochastic model of the FK spectrum.

Prior model

In order to construct a prior stochastic model for the wave field in the soil, a prior model for the dynamic soil properties is formulated first. The prior soil model reflects the knowledge on the dynamic soil properties that is available (from engineering experience or soil investigations on similar sites) before the SASW test has been performed.

The soil is modeled as a horizontally layered halfspace consisting of 8 homogeneous layers on a homogeneous halfspace. A viscoelastic material model is used where material damping is taken into account through the use of complex Lamé coefficients $\mu^* = \mu(1 + 2iD_{\mathrm{s}})$ and $(\lambda + 2\mu)^* = (\lambda + 2\mu)(1 + 2iD_{\mathrm{p}})$, where D_{s} and D_{p} represent the hysteretic material damping ratios for shear and dilatational waves, respectively.

The layer thicknesses and the elastodynamic properties of the layers and the halfspace are modeled as mutually independent lognormal variables. The mean value and the standard deviation of the layer thickness h, the shear modulus μ, the constrained modulus κ, the density ρ, and the damping ratios D_{s} and D_{p} are given in table 1. The standard deviations of the soil properties are chosen relatively large, so that their $95\,\%$ confidence regions contain the values expected at most sites in Flanders, where Heverlee is located.

Table 1. Mean value and standard deviation of the prior dynamic soil properties.

		Mean value	Standard deviation
h	[m]	2	1.5
μ	[MPa]	100	150
κ	[MPa]	250	1000
ρ	[kg/m^3]	1800	100
D_{s}	[−]	0.03	0.015
D_{p}	[−]	0.03	0.015

A Monte Carlo simulation is performed where a large number of soil profiles are generated. For each soil profile, the free field acceleration due to a vertical harmonic point load at the soil surface is computed both in the frequency-space domain and in the frequency-wavenumber domain. This leads to an ensemble of

realistic wave fields, corresponding to realistic soil profiles. The computations are performed by means of the ElastoDynamics Toolbox for MATLAB (Schevenels et al.; 2009).

The response in the frequency-space domain is computed for N_S source-receiver distances and N_F frequencies (corresponding to the distances and the frequencies in the SASW test). The results are stored in a vector $\hat{\mathbf{H}}_0$ of length $N_\mathrm{FS} = N_\mathrm{F} N_\mathrm{S}$. The response in the frequency-wavenumber domain is computed for N_K phase velocities and N_F frequencies and stored in a vector $\tilde{\mathbf{H}}_0$ of length $N_\mathrm{FK} = N_\mathrm{F} N_\mathrm{K}$. In the present analysis, $N_\mathrm{K} = 100$ non-equidistant phase velocities between $5\,\mathrm{m/s}$ and $1600\,\mathrm{m/s}$ are used. The vectors $\hat{\mathbf{H}}_0$ and $\tilde{\mathbf{H}}_0$ are concatenated, resulting in a vector $\mathbf{H}_0$ of length $N = N_\mathrm{FS} + N_\mathrm{FK}$:

$$\mathbf{H}_0 = \begin{bmatrix} \hat{\mathbf{H}}_0 \\ \tilde{\mathbf{H}}_0 \end{bmatrix} \tag{12}$$

The mean value $\mathbf{m}_{\mathbf{H}_0}$ and the covariance matrix $\mathbf{C}_{\mathbf{H}_0}$ of the vector $\mathbf{H}_0$ are subsequently determined. The mean vector $\mathbf{m}_{\mathbf{H}_0}$ is composed as follows:

$$\mathbf{m}_{\mathbf{H}_0} = \begin{bmatrix} \mathbf{m}_{\hat{\mathbf{H}}_0} \\ \mathbf{m}_{\tilde{\mathbf{H}}_0} \end{bmatrix} \tag{13}$$

where $\mathbf{m}_{\hat{\mathbf{H}}_0}$ is the mean value of the wave field $\hat{\mathbf{H}}_0$ in the frequency-space domain and $\mathbf{m}_{\tilde{\mathbf{H}}_0}$ is the mean value of the wave field $\tilde{\mathbf{H}}_0$ in the frequency-wavenumber domain. The covariance matrix $\mathbf{C}_{\mathbf{H}_0}$ is composed as follows:

$$\mathbf{C}_{\mathbf{H}_0} = \begin{bmatrix} \mathbf{C}_{\hat{\mathbf{H}}_0} & \mathbf{C}^\mathrm{H}_{\tilde{\mathbf{H}}_0 \hat{\mathbf{H}}_0} \\ \mathbf{C}_{\tilde{\mathbf{H}}_0 \hat{\mathbf{H}}_0} & \mathbf{C}_{\tilde{\mathbf{H}}_0} \end{bmatrix} \tag{14}$$

where $\mathbf{C}_{\hat{\mathbf{H}}_0}$ is the covariance matrix of the wave field $\hat{\mathbf{H}}_0$ in the frequency-space domain, $\mathbf{C}_{\tilde{\mathbf{H}}_0}$ is the covariance matrix of the wave field $\tilde{\mathbf{H}}_0$ in the frequency-wavenumber domain, and $\mathbf{C}_{\tilde{\mathbf{H}}_0 \hat{\mathbf{H}}_0}$ is the cross-covariance matrix of the vectors $\tilde{\mathbf{H}}_0$ and $\hat{\mathbf{H}}_0$.

It is assumed that the vector $\mathbf{H}_0$ follows a Gaussian distribution (which is an approximation). The probability density function $p_{\mathbf{H}_0}(\mathbf{H})$ of the vector $\mathbf{H}_0$ is then given by:

$$p_{\mathbf{H}_0}(\mathbf{H}) = \frac{1}{(2\pi)^{N/2} \left|\mathbf{C}_{\mathbf{H}_0}\right|^{1/2}} \exp\left[-\frac{1}{2} \left(\mathbf{H} - \mathbf{m}_{\mathbf{H}_0}\right)^\mathrm{H} \mathbf{C}_{\mathbf{H}_0}^{-1} \left(\mathbf{H} - \mathbf{m}_{\mathbf{H}_0}\right)\right] \tag{15}$$

Likelihood function

The likelihood function $L_{\mathbf{H}}(\mathbf{H})$ expresses how likely a wave field $\mathbf{H} = \begin{bmatrix} \hat{\mathbf{H}} \\ \tilde{\mathbf{H}} \end{bmatrix}$ is in view of the experimental data. It depends on the misfit $\Delta\hat{\mathbf{H}}$ between the transfer function $\hat{\mathbf{H}}$ and the experimental transfer function $\hat{\mathbf{H}}_\mathrm{e}$:

$$\Delta\hat{\mathbf{H}} = \hat{\mathbf{H}}_\mathrm{e} - \hat{\mathbf{H}} \tag{16}$$

The misfit $\Delta\hat{\mathbf{H}}$ consists of two terms:

$$\Delta\hat{\mathbf{H}} = \Delta\hat{\mathbf{H}}_\mathrm{e} + \Delta\hat{\mathbf{H}}_\mathrm{m} \tag{17}$$

The first term $\Delta\hat{\mathbf{H}}_\mathrm{e}$ denotes the measurement error, the second term $\Delta\hat{\mathbf{H}}_\mathrm{m}$ denotes the model error.

The measurement error $\Delta\hat{\mathbf{H}}_{\mathrm{e}}$ has been discussed in the first section; it is characterized by a zero mean value and a covariance matrix $\mathbf{C}_{\Delta\hat{\mathbf{H}}_{\mathrm{e}}} \equiv \mathbf{C}_{\hat{\mathbf{H}}_{\mathrm{e}}}$.

The model error $\Delta\hat{\mathbf{H}}_{\mathrm{m}}$ should be interpreted as a target error for the posterior model: loosely speaking, the aim of the Bayesian updating procedure is to identify all FK spectra for which the misfit with the experimental data does not exceed the model error $\Delta\hat{\mathbf{H}}_{\mathrm{m}}$. The model error is introduced in order to avoid overfitting of the experimental data, which may otherwise lead to unrealistic results. In the present analysis, the model error is assumed to be uncorrelated in terms of space and frequency. It is characterized by a zero mean value and a frequency dependent standard deviation equal to 0.2 times the maximum modulus of the experimental transfer function $\hat{\mathbf{h}}_{\mathrm{e}}(\omega)$ over all receivers. The covariance matrix $\mathbf{C}_{\Delta\hat{\mathbf{H}}_{\mathrm{m}}}$ for the model error $\Delta\hat{\mathbf{H}}_{\mathrm{m}}$ is thus equal to:

$$\mathbf{C}_{\Delta\hat{\mathbf{H}}_{\mathrm{m}}} = \begin{bmatrix} \mathbf{C}_{\Delta\hat{\mathbf{h}}_{\mathrm{m}}}(\omega_1) & & & 0 \\ & \mathbf{C}_{\Delta\hat{\mathbf{h}}_{\mathrm{m}}}(\omega_2) & & \\ & & \ddots & \\ 0 & & & \mathbf{C}_{\Delta\hat{\mathbf{h}}_{\mathrm{m}}}(\omega_{\mathrm{N_F}}) \end{bmatrix} \tag{18}$$

where the submatrices $\mathbf{C}_{\Delta\hat{\mathbf{h}}_{\mathrm{m}}}(\omega_i)$ are defined as:

$$\mathbf{C}_{\Delta\hat{\mathbf{h}}_{\mathrm{m}}}(\omega_i) = \left(0.2 \left\| \hat{\mathbf{h}}_{\mathrm{e}}(\omega_i) \right\|_{\infty}\right)^2 \mathbf{I}_{N_{\mathrm{S}}} \tag{19}$$

where $\left\| \hat{\mathbf{h}}_{\mathrm{e}}(\omega_i) \right\|_{\infty}$ is the L^{∞} norm of $\hat{\mathbf{h}}_{\mathrm{e}}(\omega_i)$ and $\mathbf{I}_{N_{\mathrm{S}}}$ is the identity matrix of size N_{S}.

Assuming that both the measurement error $\Delta\hat{\mathbf{H}}_{\mathrm{e}}$ and the model error $\Delta\hat{\mathbf{H}}_{\mathrm{m}}$ follow a Gaussian distribution, the total misfit $\Delta\hat{\mathbf{H}}$ is also Gaussian and its covariance matrix $\mathbf{C}_{\Delta\hat{\mathbf{H}}}$ is equal to:

$$\mathbf{C}_{\Delta\hat{\mathbf{H}}} = \mathbf{C}_{\Delta\hat{\mathbf{H}}_{\mathrm{e}}} + \mathbf{C}_{\Delta\hat{\mathbf{H}}_{\mathrm{m}}} \tag{20}$$

The likelihood function $L_{\mathbf{H}}(\mathbf{H})$ is finally given by:

$$L_{\mathbf{H}}(\mathbf{H}) = \frac{1}{(2\pi)^{N_{\mathrm{FS}}/2} \left|\mathbf{C}_{\Delta\hat{\mathbf{H}}}\right|^{1/2}} \exp\left[-\frac{1}{2}\left(\hat{\mathbf{H}}_{\mathrm{e}} - \hat{\mathbf{H}}\right)^{\mathrm{H}} \mathbf{C}_{\Delta\hat{\mathbf{H}}}^{-1}\left(\hat{\mathbf{H}}_{\mathrm{e}} - \hat{\mathbf{H}}\right)\right] \tag{21}$$

Posterior model

According to Bayes' theorem 1763, the posterior probability distribution $p_{\mathbf{H}}(\mathbf{H})$ of the wave field $\mathbf{H}$ in the soil is given by:

$$p_{\mathbf{H}}(\mathbf{H}) = \frac{1}{k} p_{\mathbf{H}_0}(\mathbf{H}) L_{\mathbf{H}}(\mathbf{H}) \tag{22}$$

where k is a normalization constant introduced to ensure that the function $p_{\mathbf{H}}(\mathbf{H})$ integrates to one.

Since both the prior probability distribution $p_{\mathbf{H}_0}(\mathbf{H})$ and the likelihood function $L_{\mathbf{H}}(\mathbf{H})$ are Gaussian, the posterior probability distribution $p_{\mathbf{H}}(\mathbf{H})$ is also Gaussian:

$$p_{\mathbf{H}}(\mathbf{H}) = \frac{1}{(2\pi)^{N/2} \left|\mathbf{C}_{\mathbf{H}}\right|^{1/2}} \exp\left[-\frac{1}{2}\left(\mathbf{H} - \mathbf{m}_{\mathbf{H}}\right)^{\mathrm{H}} \mathbf{C}_{\mathbf{H}}^{-1}\left(\mathbf{H} - \mathbf{m}_{\mathbf{H}}\right)\right] \tag{23}$$

where the mean vector $\mathbf{m}_{\mathbf{H}}$ and the covariance matrix $\mathbf{C}_{\mathbf{H}}$ are composed as follows:

$$\mathbf{m}_{\mathbf{H}} = \begin{bmatrix} \mathbf{m}_{\hat{\mathbf{H}}} \\ \mathbf{m}_{\tilde{\mathbf{H}}} \end{bmatrix} \tag{24}$$

$$\mathbf{C}_{\mathbf{H}} = \begin{bmatrix} \mathbf{C}_{\hat{\mathbf{H}}} & \mathbf{C}_{\tilde{\mathbf{H}}\hat{\mathbf{H}}}^{\mathrm{H}} \\ \mathbf{C}_{\tilde{\mathbf{H}}\hat{\mathbf{H}}} & \mathbf{C}_{\tilde{\mathbf{H}}} \end{bmatrix} \tag{25}$$

The submatrices of interest are the mean value $\mathbf{m}_{\tilde{\mathbf{H}}}$ and the covariance $\mathbf{C}_{\tilde{\mathbf{H}}}$ of the posterior wave field $\tilde{\mathbf{H}}$ in the frequency-wavenumber domain. These can be determined analytically (Anderson and Moore; 1979) by equating the right hand sides of equations (22) and (23):

$$\mathbf{m}_{\tilde{\mathbf{H}}} = \mathbf{m}_{\tilde{\mathbf{H}}_0} + \mathbf{B}\left(\hat{\mathbf{H}}_\mathrm{e} - \mathbf{m}_{\hat{\mathbf{H}}_0}\right) \tag{26}$$

$$\mathbf{C}_{\tilde{\mathbf{H}}} = \mathbf{C}_{\tilde{\mathbf{H}}_0} - \mathbf{B}\mathbf{C}^{\mathrm{H}}_{\tilde{\mathbf{H}}_0\hat{\mathbf{H}}_0} \tag{27}$$

where $\mathbf{B}$ is the Kalman gain matrix:

$$\mathbf{B} = \mathbf{C}_{\tilde{\mathbf{H}}_0\hat{\mathbf{H}}_0}\left(\mathbf{C}_{\hat{\mathbf{H}}_0} + \mathbf{C}_{\hat{\mathbf{H}}_\mathrm{e}}\right)^{-1} \tag{28}$$

The variance $\boldsymbol{\sigma}^2_{\tilde{\mathbf{H}}}$ of the posterior FK spectrum is obtained as:

$$\boldsymbol{\sigma}^2_{\tilde{\mathbf{H}}} = \mathrm{diag}\left(\mathbf{C}_{\tilde{\mathbf{H}}}\right) \tag{29}$$

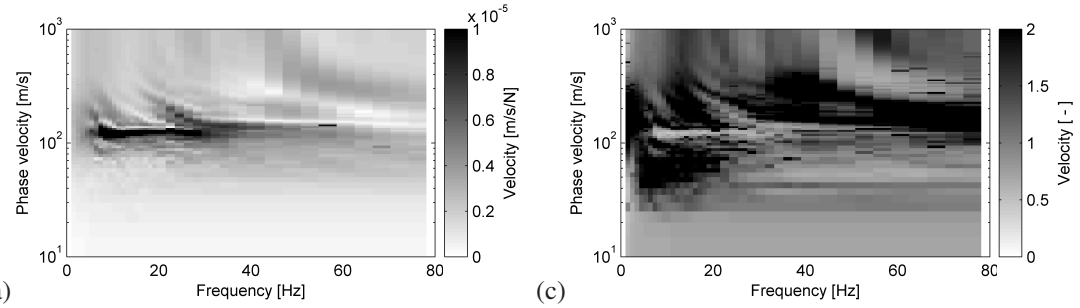

Figure 2. (a) Mean value $|\mathbf{m}_{\tilde{\mathbf{H}}}|$ and (b) coefficient of variation $\boldsymbol{\sigma}_{\tilde{\mathbf{H}}}/|\mathbf{m}_{\tilde{\mathbf{H}}}|$ of the FK spectrum for the site in Heverlee.

Figure 2 shows the modulus of the mean value $\mathbf{m}_{\tilde{\mathbf{H}}}$ and the coefficient of variation $\boldsymbol{\sigma}_{\tilde{\mathbf{H}}}/|\mathbf{m}_{\tilde{\mathbf{H}}}|$ of the posterior FK spectrum. Figure 2a clearly reveals the contribution of the fundamental Rayleigh mode to the response at the soil surface, resulting in a peak in the FK spectrum. Additional peaks corresponding to higher modes can also be distinguished. As the posterior FK spectrum follows a Gaussian distribution, the mean FK spectrum $\mathbf{m}_{\tilde{\mathbf{H}}}$ shown in figure 2a is the spectrum with maximum posterior probability. From a deterministic point of view, it can therefore be considered as the one and only true FK spectrum for the site in Heverlee.

The coefficient of variation $\boldsymbol{\sigma}_{\tilde{\mathbf{H}}}/|\mathbf{m}_{\tilde{\mathbf{H}}}|$ of the posterior FK spectrum shown in figure 2c is relatively large over the entire range of frequencies and phase velocities, except for the frequencies between $6\,\mathrm{Hz}$ and $40\,\mathrm{Hz}$ and the phase velocities corresponding to the Rayleigh modes. It can therefore be concluded that the SASW test performed in Heverlee allows for an accurate determination of the dispersion and attenuation curves between $6\,\mathrm{Hz}$ and $40\,\mathrm{Hz}$. At lower frequencies, the wavelength of the waves in the soil is large compared to the array length; as a consequence, the waves are not properly resolved by the receivers, resulting in a low accuracy of the FK spectrum. At higher frequencies, the wavelength is small compared to the distance between adjacent receivers, leading to spatial aliasing and a low accuracy of the FK spectrum.

INVERSION

This section focuses on the determination of the dynamic soil properties, using the FK spectrum obtained in the previous section. A Bayesian approach is followed in order to determine the soil profile(s) matching the FK spectrum. In contrast to the Bayesian updating procedure used to determine the FK spectrum, the

present updating cannot be performed analytically due to (1) the non-Gaussian character of the dynamic soil properties and (2) the non-linear relation between the dynamic soil properties (the model parameters) and the FK spectrum (the observations). A Markov chain Monte Carlo procedure is therefore used instead, resulting in an ensemble of soil profiles that correspond well to the experimental FK spectrum.

Prior model
First a prior model for the dynamic soil properties is formulated. This model is identical to the soil model that has been used in the previous section to determine a prior model for the wave field in the soil.

Likelihood function
The likelihood function is formulated in terms of the FK spectrum of the soil. For each conceivable soil profile, the FK spectrum $\tilde{\mathbf{H}}$ can be computed. The likelihood function $L(\tilde{\mathbf{H}})$ is then a measure for the similarity between this spectrum $\tilde{\mathbf{H}}$ and the experimental FK spectrum determined in the previous section. As the experimental FK spectrum follows a Gaussian distribution, the likelihood function $L(\tilde{\mathbf{H}})$ is given by:

$$L(\tilde{\mathbf{H}}) = \frac{1}{(2\pi)^{N_{\mathrm{FK}}/2} \left|\mathbf{C}_{\tilde{\mathbf{H}}}\right|^{1/2}} \exp\left[-\frac{1}{2}\left(\tilde{\mathbf{H}} - \mathbf{m}_{\tilde{\mathbf{H}}}\right)^{\mathrm{H}} \mathbf{C}_{\tilde{\mathbf{H}}}^{-1}\left(\tilde{\mathbf{H}} - \mathbf{m}_{\tilde{\mathbf{H}}}\right)\right] \tag{30}$$

Posterior model
The posterior soil model is determined by means of a Markov chain Monte Carlo procedure. This procedure yields an ensemble of soil profiles following the posterior probability distribution. The procedure is described in detail in reference (Schevenels et al.; 2008), where it is also applied in the context of the SASW method, using the dispersion curve for the determination of the soil properties instead of the FK spectrum.

From the ensemble of soil profiles obtained, the soil profile with maximum posterior probability can be considered as the solution to the inverse problem. This profile is shown in figure 3, together with five other profiles randomly taken from the ensemble.

The soil profile with maximum posterior probability shown in figure 3 appears as a realistic solution, except for the high damping ratio D_{s} at the surface and the relatively low value of the the dilatational wave velocity C_{p} (compared to the shear wave velocity C_{s}) at larger depths. The occurrence of such unrealistic features can be suppressed by modifying the prior soil model. The high value of the damping ratio can be avoided through the use of e.g. a uniform probability distribution with bounds at 0.01 and 0.1 (to reflect that values below 0.01 and above 0.1 are unrealistic). The low value of the dilatational wave velocity C_{p} can be avoided in a similar way by using a realistic lower bound for the constrained modulus κ in the prior soil model.

The five other profiles shown in figure 3 are drawn from the posterior soil model, which implies that they also correspond well to the experimental FK spectrum. The variability of these profiles illustrates the non-unique character of the solution to the inverse problem. The shear wave velocity shown in figure 3a is relatively well resolved, resulting in a relatively low variability of the solution. The variability of the other soil properties is higher. Taking into account that the standard deviation of the density is only $100\,\mathrm{kg/m^3}$ in the prior soil model, the variability of the posterior density in figure 3e is very high, which confirms that the SASW test cannot be used to determine the density of the soil.

Figures 3a and 3b also show the shear wave velocity C_{s} and the dilatational wave velocity C_{p} as obtained from a Seismic Cone Penetration Test (SCPT) performed at the same site (Areias; 2009). The shear wave velocity profiles obtained with the SASW method and the SCPT method correspond very well (figure 3a), except at small depths (less than $2\,\mathrm{m}$) and at large depths (more than $10\,\mathrm{m}$). Possible explanations are the limited resolution of the SCPT at small depths and the SASW test at large depths, or local variations of

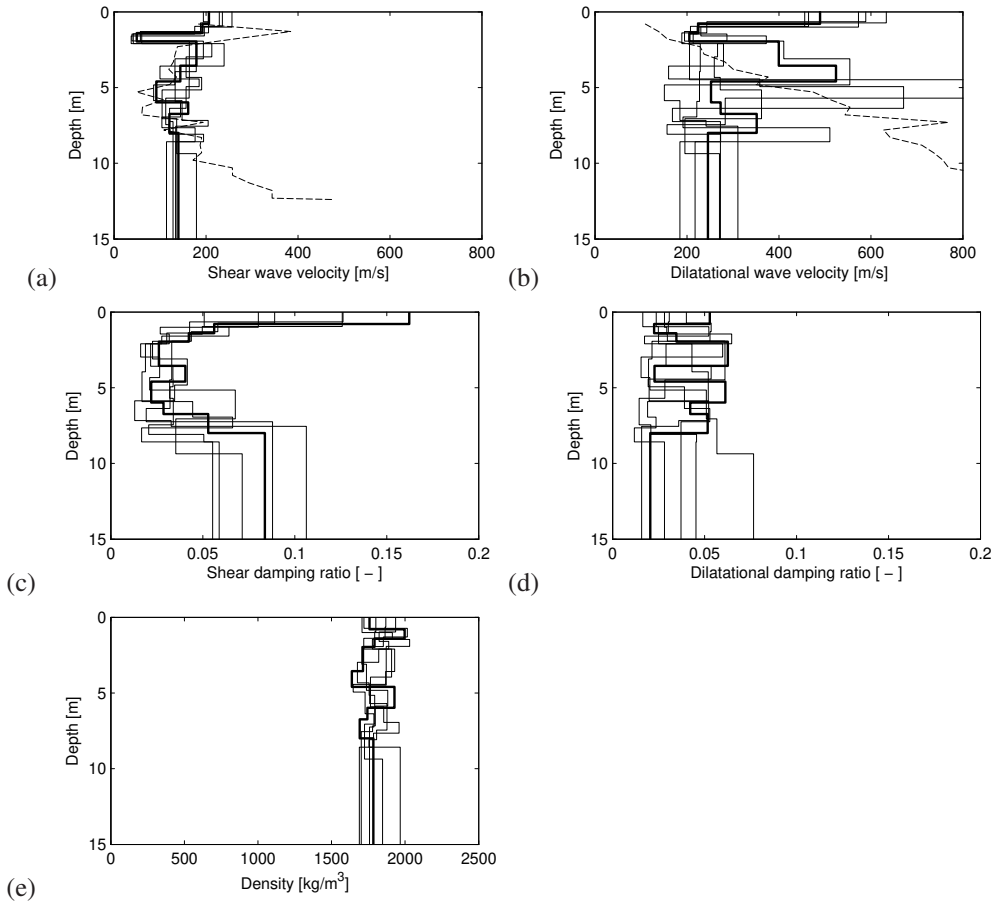

Figure 3. (a) Shear wave velocity C_{s}, (b) dilatational wave velocity C_{p} (c) material damping ratio D_{s} for shear waves, (d) material damping ratio D_{p} for dilatational waves, and (e) density ρ as a function of depth at the site in Heverlee. The thick solid line is the soil profile with maximum posterior probability, the thin solid lines are five randomly selected profiles from the ensemble obtained with the Markov chain Monte Carlo method, and the dashed line is a profile obtained with the SCPT method.

the soil properties that are detected by the SCPT method but not by the SASW method. The dilatational wave velocity profiles obtained with both methods are different (figure 3b), which may be explained by the non-uniqueness of the profile obtained with the SASW method.

VERIFICATION

In order to verify the identified soil profile, it is used to simulate the transfer function between the hammer force and the free field response. The simulation is performed for the soil profile with maximum posterior probability as well as the five other soil profiles shown in figure 3. The results are compared with the experimental data shown in figure 1.

Figure 4 compares the computed and experimental transfer function for four different receivers. The correspondence between the computed and experimental data is satisfactory, indicating that the soil profile obtained properly reflects the experimental data. This holds for the soil profile with maximum posterior probability, but also for the other selected soil profiles, again illustrating the non-uniqueness of the solution to the inverse problem: a large variety of soil profiles can be found that are compatible with the measurement data, making it impossible to determine the actual soil properties.

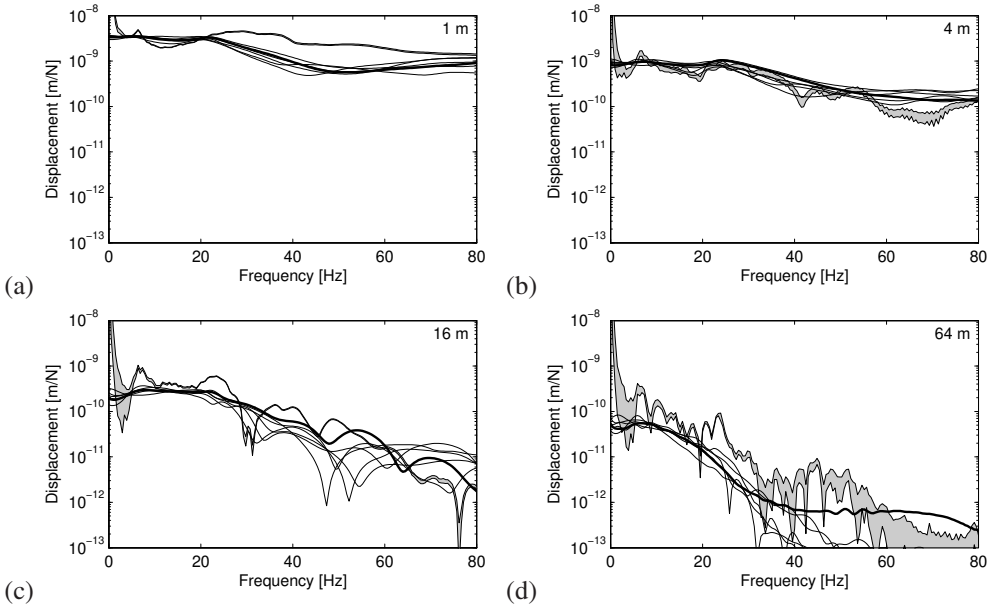

Figure 4. Modulus of the transfer function between the hammer force and the free field displacement at (a) $1\,\mathrm{m}$**, (b)** $4\,\mathrm{m}$**, (c)** $16\,\mathrm{m}$**, and (d)** $64\,\mathrm{m}$ **from the source. The thick line is the transfer function computed using the soil profile with maximum posterior probability, the thin lines correspond to the five other soil profiles shown in figure 3, and the gray region is the** $95\,\%$ **confidence region of the experimental transfer function.**

CONCLUSION

This paper presents a Bayesian approach for the determination of the FK spectrum in SASW tests. A prior model is formulated for the wave field in the soil, based on a Monte Carlo simulation where the wave field is computed for a large number of realistic soil profiles. This model is updated using the data obtained from the SASW test in order to obtain a posterior model for the wave field. The updating is performed by means of an analytical technique closely related to the Kalman filter.

The advantage of this approach compared to integral transformation methods is that it avoids the (linear) interpolation of the wave field between the sensor locations and truncation of the integral at the array length, both leading to artifacts in the FK spectrum. Moreover, the proposed method yields a complete stochastic description of the FK spectrum, which can be used in a stochastic inversion procedure for the determination of the dynamic soil properties.

The approach presented in the paper is applied to a data set collected from an SASW test performed in Heverlee (Belgium). The resulting FK spectrum is used to detemine the soil profile by solving an inverse problem, following a Markov chain Monte Carlo procedure. The soil profile with maximum posterior probability is considered as the solution to the inverse problem. In order to verify the soil profile obtained, a simulation is performed of the transfer function between the impact force and the free field response measured in the SASW test. A good correspondence between the computed transfer function and the experimental data is observed. This implies that the soil profile obtained is compatible with the experimental data and thus illustrates the applicability of the proposed method in a realistic scenario.

ACKNOWLEDGEMENTS

The first author is a postdoctoral fellow of the Research Foundation - Flanders. The financial support is gratefully acknowledged.

REFERENCES

Anderson, B. and Moore, J. (1979). *Optimal filtering*, Prentice Hall, Englewood Cliffs, NJ.

Areias, L. (2009). Seismic cone test SCPT1, Arenberg III campus, Celestijnenlaan, Heverlee, *Technical report*, Laboratorium voor Geotechniek, UGent.

Badsar, S., Schevenels, M., Haegeman, W. and Degrande, G. (2010). Determination of the damping ratio in the soil from SASW tests using the half-power bandwidth method, *Geophysical Journal International* **182**(3): 1493–1508.

Bayes, T. (1763). An essay towards solving a problem in the doctrine of chances, *Philosophical Transactions of the Royal Society* **53**: 370–418.

Cauberghe, B. (2004). *Applied frequency-domain system identification in the field of experimental and operational modal analysis*, PhD thesis, Vrije Universiteit Brussel.

Cuellar, V. and Valerio, J. (1997). Use of the SASW method to evaluate soil improvement techniques, *Proceedings of the 14th international conference soil mechanics and foundation engineering*, Hamburg, pp. 461–464.

Databank Ondergrond Vlaanderen (2010). http://dov.vlaanderen.be.

Ewins, D. (1984). *Modal testing: theory and practice*, Research Studies Press Ltd., Letchworth, UK.

Forbriger, T. (2003a). Inversion of shallow-seismic wavefields: I. Wavefield transformation, *Geophysical Journal International* **153**(3): 719–734.

Forbriger, T. (2003b). Inversion of shallow-seismic wavefields: II. Inferring subsurface properties from wavefield transforms, *Geophysical Journal International* **153**(3): 735–752.

Kavazanjian, E., Snow, M., Poran, C. and Satoh, T. (1994). Non-intrusive Rayleigh wave investigations at solid waste landfills, *Proceedings of the first international congress on environmental geotechnics*, Edmonton, pp. 707–712.

Lai, C. (1998). *Simultaneous inversion of Rayleigh phase velocity and attenuation for near-surface site characterization*, PhD thesis, Georgia Institute of Technology.

Lombaert, G., Degrande, G., Kogut, J. and François, S. (2006). The experimental validation of a numerical model for the prediction of railway induced vibrations, *Journal of Sound and Vibration* **297**(3-5): 512–535.

Maraschini, M. and Foti, S. (2010). A Monte Carlo multimodal inversion of surface waves, *Geophysical Journal International* **182**(3): 1557–1566.

Mosegaard, K. and Tarantola, A. (1995). Monte Carlo sampling of solutions to inverse problems, *Journal of Geophysical Research* **100**: 12431–12447.

Nazarian, S. and Desai, M. (1993). Automated surface wave method: field testing, *Journal of Geotechnical Engineering, Proceedings of the ASCE* **119**(7): 1094–1111.

Nazarian, S. and Stokoe II, K. (1984). Nondestructive testing of pavements using surface waves, *Transportation Research Record* **993**: 67–79.

Rix, G., Lai, C. and Spang Jr., A. (2000). In situ measurement of damping ratio using surface waves, *Journal of Geotechnical and Geoenvironmental Engineering, Proceedings of the ASCE* **126**(5): 472–480.

Schevenels, M. and Degrande, G. (2009). Site vibration evaluation on the Arenberg III campus for the planning of a nanotechnology laboratory, *Technical Report BWM-2009-04*, Department of Civil Engineering, K.U.Leuven.

Schevenels, M., François, S. and Degrande, G. (2009). EDT: An ElastoDynamics Toolbox for MATLAB, *Computers & Geosciences* **35**(8): 1752–1754.

Schevenels, M., Lombaert, G., Degrande, G. and François, S. (2008). A probabilistic assessment of resolution in the SASW test and its impact on the prediction of ground vibrations, *Geophysical Journal International* **172**(1): 262–275.

Yuan, D. and Nazarian, S. (1993). Automated surface wave method: inversion technique, *Journal of Geotechnical Engineering, Proceedings of the ASCE* **119**(7): 1112–1126.